Shape-Controlled Synthesis of Pt Nanocrystals: The Role of Metal Carbonyls

Yijin Kang,[†] Jun Beom Pyo,[‡] Xingchen Ye,[†] Rosa E. Diaz,[§] Thomas R. Gordon,[†] Eric A. Stach,[§] and Christopher B. Murray[†,‡,*]

[†]Department of Chemistry and [‡]Department of Materials Science and Engineering, University of Pennsylvania, Philadelphia, Pennsylvania 19104, United States, and [§]Center for Functional Nanomaterials, Brookhaven National Laboratory, Upton, New York 11973, United States

ABSTRACT Well-controlled synthesis of nanocrystals is necessary to unambiguously correlate the structural properties of nanocrystals with the catalytic properties. The most common low-index surfaces are (111) and (100). Therefore, model materials with {111} and {100} facets are highly desirable, in order to understand the catalytic properties of (111) and (100) surfaces for various structure-sensitive reactions. We report a solution-phase synthesis using metal carbonyls as additives. This synthetic method produces highly monodisperse Pt octahedra and icosahedra as the model of Pt{111}, Pt cubes as the model of Pt{100}, respectively. Several other morphologies, such as truncated cubes, cuboctahedra, spheres, tetrapods, star-shaped octapods, multipods, and hyper-branched structure, are produced, as well. A bifunctional role of metal carbonyl in the synthesis is identified: zerovalent transition metal decomposed from metal carbonyl acts as a shape-directing agent, while CO provides the reducing power. These high-quality shape-controlled Pt nanocrystals are suitable for model catalyst studies.

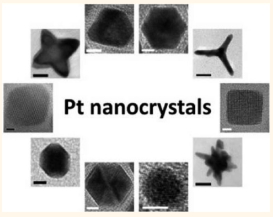

KEYWORDS: platinum · nanocrystal · shape control · morphology · catalysis · electrocatalysis · CO oxidation

Material synthesis is at the core of the ever evolving field of nanoscience.[1] Size- and shape-controlled synthesis are of great interest,[2−10] due to many applications where nanocrystal surface structure influences material or device performance, namely, in catalysis,[9,11−21] optics,[22−25] magnetics,[26−28] and electronics.[29] The shape-controlled synthesis of Pt nanocrystals, pioneered by El-Sayed *et al.*,[30] has been most thoroughly explored for applications in catalysis, as the structure effect in heterogeneous catalysis has long been recognized[31−39] (*e.g.*, ammonia synthesis over Fe surface,[33] ethane hydrogenolysis over Ni and Pt,[34] and heptane dehydrocyclization over Pt[31]). Similarly, a number of reactions are shown to be structure-sensitive on nanocrystals. For instance, Feliu *et al.* have reported shape-dependent methanol and formic acid electrooxidation on preferentially oriented Pt nanoparticles;[13] Zaera *et al.* have demonstrated tunable selectivity for isomerization reactions by controlling the particle shape of Pt;[40] and Somorjai *et al.* have shown the shape effects for benzene hydrogenation on Pt nanocrystals.[11]

Well-controlled synthesis of nanocrystals is necessary to unambiguously correlate structure with catalytic properties. While shape control at the scale of tens of nanometers up to hundreds of nanometers has been successfully achieved for many systems,[2,3,41,42] the synthesis of well-controlled Pt nanocrystals under 20 nm in size remains challenging. In this report, we describe the preparation of highly monodisperse Pt nanocrystals ($\sigma < 6\%$) with a variety of morphologies through solution-phase synthesis.

This synthesis of Pt nanocrystals utilizes Pt acetylacetonate [$Pt(acac)_2$] as a Pt source, oleic acid and oleylamine as capping agents (oleylamine is also a cosolvent, in addition to the benzyl ether), and metal carbonyls as additives (or shape-directing agents). In previous research, it is observed that by reducing the amount of metal carbonyls in solution, pure Pt nanocubes are isolated rather than Pt-based alloy nanocubes,[15,43,44] and that the Pt nanocubes can be synthesized using CO as reducing agent, in the absence of metal carbonyls.[15] In this work, we experiment with various solvents in which the metal carbonyls are dissolved prior to

* Address correspondence to cbmurray@sas.upenn.edu.

Received for review October 18, 2012 and accepted December 4, 2012.

Published online December 04, 2012
10.1021/nn3048439

injection. Interestingly, we notice that, by using chloroform, pure Pt nanocrystals are generated, while other solvents (benzyl ether, hexane, dichlorobenzene, toluene, *etc.*) produce Pt-based alloys. In addition, when chloroform is used, ammonium chloride is produced as a major byproduct. Recognizing that chloroform can inhibit the foreign metal from forming an alloy with Pt, we use a chloroform solution of dimanganese decacarbonyl as additive agent to control the shape of Pt nanocrystals.

RESULTS AND DISCUSSION

Pt Nanocrystals Enclosed by {111} Facets. A Pt nanocrystal is primarily enclosed with {111} and {100} facets, due to the low surface energies associated with these facets. As a result, model materials with {111} and {100} facets are highly desirable, in order to understand the catalytic properties of {111} and {100} planes on the surface of catalysts in structure-sensitive reactions. High percentages of {100} facets are readily achieved since highly uniform Pt nanocubes exposing {100} facets have been reported using several available methods.[11,15,43−48] In contrast, preparation of nanocrystals with primarily {111} facets has been challenging, although preferentially {111}-exposed Pt nanoparticles have been produced by several leading groups.[13,47] Here, we present the synthesis of two morphologies of highly controlled Pt nanocrystals which present primarily (111) surfaces: Pt octahedra and Pt icosahedra.

Pt octahedra are synthesized *via* the reduction of $Pt(acac)_2$ initiated by the injection of a chloroform solution of $Mn_2(CO)_{10}$, in the presence of oleic acid and oleylamine. The atomic ratio of Mn/Pt in the precursor is 1/5. However, the concentration of Mn is less than 1% (atomic) in the final product (by ICP-OES), thus the final product of octahedra can be considered to be pure Pt octahedra. The Pt octahedra have a size of 12.56 ± 0.36 nm (vertex-to-vertex) and readily assemble to form a Minkowski lattice-type superlattice,[41] as shown in Figure 1. The aberration-corrected HRTEM image of a single Pt octahedra shown in Figure 1d reveals interplanar distances in the range of 0.222 to 0.226 nm, which is consistent with the lattice spacing of 0.227 nm for the {111} planes of the fcc platinum structure (Figure 1d). The measured angle between two facets is about 109°, which is close to the dihedral angle of octahedra which is 109.5°. As shown in the HRTEM image (Figure 1d), the observed {111} planes are parallel to the surfaces of Pt octahedra, indicating that the facets at the surface are also {111}. All of these together confirm the octahedral shape of the Pt nanocrystals, as the HRTEM image is the projection of the octahedral model down the [110] zone axis (Figure 1d). Attempts are made to tune the size of the Pt octahedra by changing the Pt/Mn ratio, Pt/ligands ratio, reaction time, and reaction temperature. However, thus far,

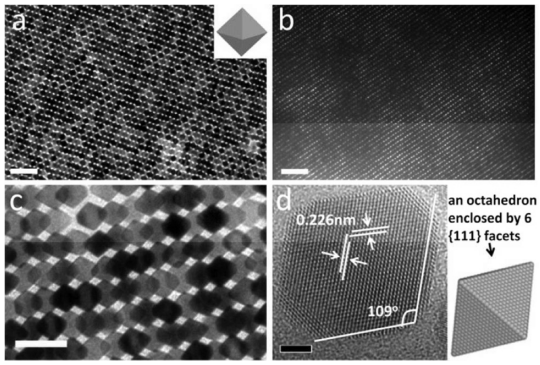

Figure 1. (a−c) TEM images and (d) HRTEM images of Pt octahedra and (a) a superlattice and (b) a 3D superlattice formed from the Pt octahedra. Scale bars: (a,b) 50 nm, (c) 20 nm, (d) 2 nm.

these reactions result in the preparation of Pt nanocrystals with other morphologies which are described in following paragraphs, thus the size of the Pt octahedra is not readily tunable in this system.

During the purification and characterization of the Pt octahedra, we observe that Pt icosahedra are also produced as a byproduct in varying quantities, depending on the synthetic conditions. An icosahedron is an alternative shape in which only {111} facets are exposed. However, an icosahedron has a multi-twinned structure, in which 20 fcc-structured single-crystalline tetrahedra share one apex. Such multi-twinned structures may result in other interesting properties due to their complex structure. While icosahedra of Fe, Pd, Au, Ag, and alloys have been prepared previously,[49−55] to the best of our knowledge, synthesis of Pt icosahedra has not been reported to date. Here, we modify and optimize the synthesis to produce high-quality icosahedra.

Although the Pt icosahedra produced during the synthesis of Pt octahedra can easily be collected through a size-selective precipitation, the yield is too low to be used as a routine synthetic method to prepare Pt icosahedra. Literature reports suggest that the growth of multi-twinned nanocrystals is a kinetically controlled process under slow reaction conditions.[49] Therefore, reducing the overall reaction rate may favor the growth of icosahedra, which can be achieved by simply lowering the reaction temperature. Because the minimum temperature at which the Pt precursor may be decomposed and reduced to Pt^0 is approximately 180 °C, we adjust the temperature to 190 °C while retaining the other synthetic parameters used in the synthesis of Pt octahedra. The yield of Pt icosahedra is increased to ∼50% (particle number), while the remaining product consists of truncated cubes and/or cuboctahedra. Since the particle size is much larger, the Pt icosahedra are less soluble in hexane than the other Pt nanocrystals. Simply washing the product mixture with hexane (containing 1% oleylamine) can effectively purify the Pt icosahedra (Figure 3). After the purification process, the purity (in terms of shape) of

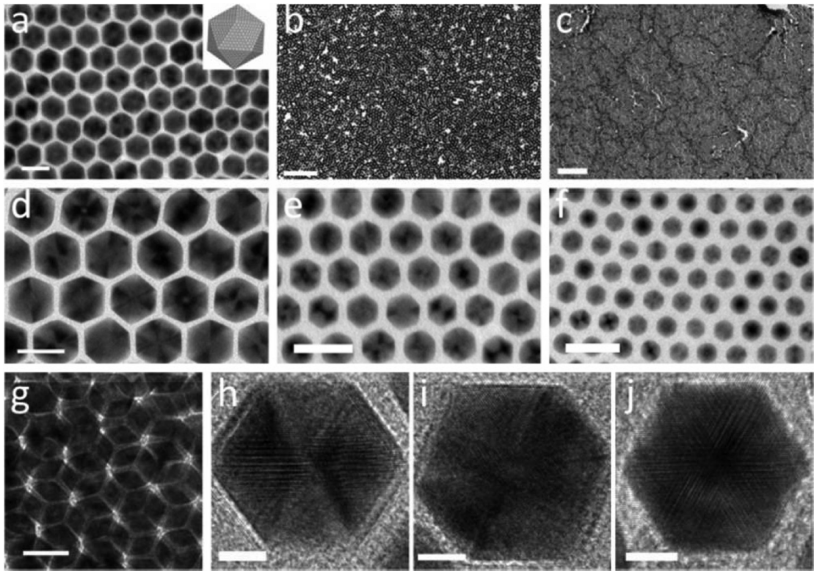

Figure 2. (a−g) TEM and (h−j) HRTEM images of Pt icosahedra. (a) Typical Pt icosahedra; (b,c) Pt icosahedra over a large area; (d−f) size of Pt icosahedra is tunable: (d) 20.43 nm, (e) 11.92 nm, (f) 8.07 nm; (g) Pt icosahedra in a self-assembly behave as semihard spheres; (h−j) HRTEM images show the distinctive pattern for the morphology of icosahedra. Scale bars: (a,d−g) 20 nm, (b) 200 nm, (c) 1 μm, (h−j) 5 nm.

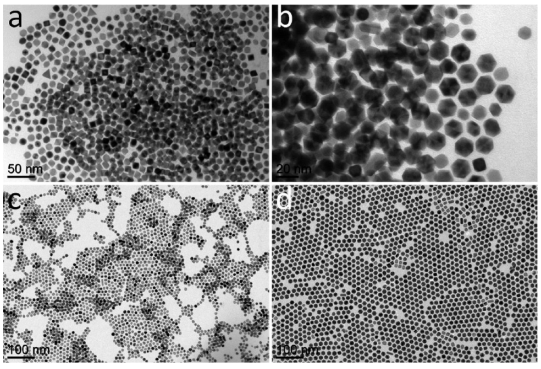

Figure 3. TEM images showing (a) the presence of Pt icosahedra as a major byproduct in the synthesis; (b) the coexistence of icosahedra and cuboctahedra in a product mixture from the optimized synthesis; (c) the cuboctahedra and (d) the icosahedra separated from the product mixture.

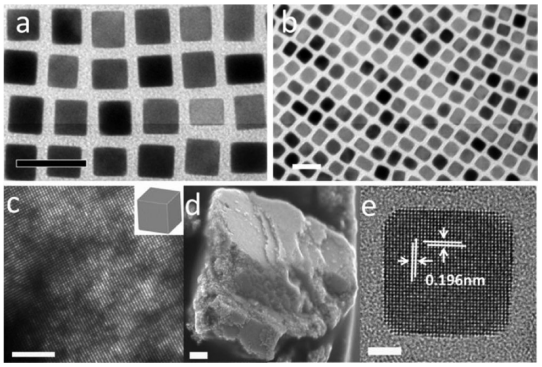

Figure 4. (a−c) TEM, (d) SEM, and (e) HRTEM images of Pt nanocubes. (a) Pt nanocubes synthesized using CO as reducing agent; (b) Pt nanocubes obtained using $Mn_2(CO)_{10}$ at 240 °C; (c) large-area superlattice and (d) supercrystal can be made by self-assembly of high-quality Pt nanocubes; (e) HRTEM image confirms that the facets of Pt nanocubes are Pt(100). Scale bars: (a,b) 20 nm, (c,d) 200 nm, (e) 2 nm.

Pt icosahedra can reach as high as 98% (~500 nanocrystal counts), as shown in Figure 2. TEM images (Figure 2a−d) indicate a high degree of monodispersity (σ < 5%) of the Pt icosahedra with the size of 20.43 ± 0.13 nm (shortest vertex-to-vertex distance). The unique interference patterns shown in HRTEM images (Figure 2h−j) are a distinctive characteristic of icosahedra, as described in literature.[51] The size of Pt icosahedra is tunable through the use of other metal carbonyls, which affects the reaction rate. For example, the Pt icosahedra synthesized with $Re_2(CO)_{10}$ instead of $Mn_2(CO)_{10}$ are smaller, having a size of 11.92 ± 0.36 nm (Figure 2e), and the Pt icosahedra as a byproduct separated from Pt octahedra synthesis have a size of 8.07 ± 0.23 nm (Figure 2f).

Pt Nanocrystals Enclosed by {100} Facets. Pt nanocubes exposing {100} facets can be synthesized using CO as reducing agent or by employing a reduced amount of Mn carbonyl. Using CO as reducing agent produces Pt cubes which are very uniform in shape but possess a larger size distribution when compared to using Mn carbonyl. In order to assemble nanocubes produced using CO into the superlattices or supercrystals, as shown in Figure 4c,d, further purification steps are necessary. On the other hand, although the size is more uniform, a Mn−Pt alloy phase may be involved in the initial nucleation stage during the synthesis of Pt nanocubes involving Mn carbonyl, thus the final product is inevitably contaminated by some amount of Mn, which may be an issue for some applications. Nevertheless, the Pt nanocubes prepared through these two methods are as good as, or better than, those reported in literature.

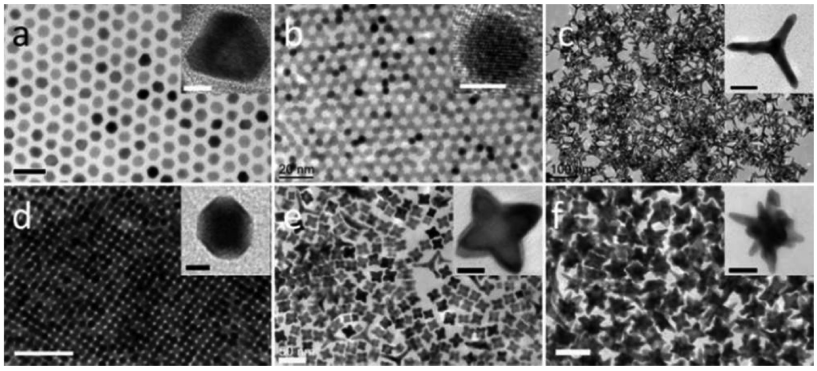

Figure 5. TEM images of (a) Pt cuboctahedra, (b) Pt spheres, (c) Pt tetrapods, (d) Pt truncated cubes, (e) Pt star (octapods), (f) Pt multipods. Scale bars: (a,b) 20 nm, (c) 100 nm, (d–f) 50 nm, insets of (a,b,d) 5 nm, insets of (c,f) 20 nm, and inset of (e) 10 nm.

As shown in the aberration-corrected HRTEM images (Figure 4e), the interplanar distances measured are in the range of 0.196–0.198 nm, which correlate with the lattice spacing for the {200} planes of Pt (0.196 nm). In addition, we observe that the edges of Pt nanocubes are parallel to {200} planes, confirming that Pt nanocubes are terminated by Pt(100). It is worth noting that the same recipe used to synthesize Pt octahedra also produces cubes at temperatures above 240 °C (Figure 4b), instead of Pt octahedra.

Other Morphologies of Pt Nanocrystals. Pt nanocrystals of other morphologies can be obtained through the use of Mn carbonyl, as shown in Figure 5. By increasing Mn/Pt ratio to 1:1, Pt cuboctahedra with a size of 7.03 ± 0.35 nm (shortest vertex-to-vertex distance) can be synthesized (Figure 5a). By further increasing the Mn/Pt ratio to 2:1, near spherical Pt nanocrystals with a size of 4.68 ± 0.20 nm (diameter) are produced (Figure 5b).

As mentioned previously, when the concentration of Mn carbonyl is kept constant and the reaction temperature is reduced, mixtures of truncated cubes (or cuboctahedra) and icosahedra are produced. The lower temperature (*i.e.*, ~190 °C) favors the formation of truncated cubes, while cuboctahedra are preferentially produced at slightly higher temperature (*i.e.*, ~200 °C). In reality, both of these two shapes are "truncated" cubes. When the edge lengths of {100} facets are equal to that of {111} facets, the shape is usually referred to as cuboctahedron; when the degree of truncation (in the ⟨111⟩ direction) is less than a cuboctahedron has, the shape is defined as truncated cube. After separating icosahedra from the mixture, the Pt cuboctahedra are of similar quality to the sample shown in Figure 5a, while Figure 5d presents the typical Pt truncated cubes.

In the synthesis of Mn–Pt nanocubes, tetrapods are observed. The elemental analysis by ICP-OES indicates that such tetrapods are nearly pure Pt (>98%). When the shape of Pt nanocrystals is monitored during the growth, we observe that concave Mn–Pt nanocubes form at early stage of the growth of Mn–Pt nanocubes, similar to the observation in the growth of Pt–Cu nanocubes.[56] During this stage, small amounts of pyramids are also formed, most likely as the incomplete cubes. While the Mn–Pt concave cubes grow into nanocubes, the pyramids gradually grow into tetrapods from the four apexes (Figure S1 in Supporting Information). The yield of tetrapods is usually so low that they are overlooked under many circumstances. The origin of such growth of tetrapods has not been identified, thus the optimized synthesis for the tetrapods has not been developed. Nonetheless, as shown in Figure 5c, the tetrapods can be separated from major product by the size-selective precipitation (tetrapods remain in the precipitate). For some applications in which the quantity of materials is not the limiting factor, this preparation of Pt tetrapods that relies on the separation could be used.

By reducing the amount of Mn carbonyl (in benzyl ether) to Mn/Pt = 1:5, pure Pt nanocubes (>99%) are produced rather than Mn–Pt alloy nanocubes. By further decreasing the Mn/Pt ratio to below 1:10 or increasing the reaction time from 15 to 30 min, Pt stars (octapods) and multipods are produced (Figure 5e,f). The octapods and multipods usually coexist; lower reaction temperature favors the formation of more multipods over the star-shaped octapods. For instance, a reaction at 220 °C preferentially produces octapods; the multipods become major product at 200 °C. If the reaction time is increased from 30 to 90 min, the branches of Pt nanocrystals can further grow to produce a spike-like hyper-branched structure (Figure 6).

Discussion of Possible Mechanisms. Putting all of the syntheses together, we find some general trends, and possible mechanisms are discussed here. The use of chloroform is the key to avoid the formation of a Mn–Pt alloy phase even at a Mn/Pt ratio as high as 2:1, and NH_4Cl forms as one major byproduct in these reactions (Figure S2). Oleylamine is the only source of N, and the chloroform is the only source of Cl. However, to the best of our knowledge, the reaction of amine and chloroform to produce NH_4Cl is not a known process. Thus, this process is not completely clear.

In this reported synthetic system, the role of $Mn_2(CO)_{10}$ has been investigated, as it is used in most of the syntheses. Previously, we discussed the connection

between $Mn_2(CO)_{10}$ and CO, namely, that CO acts as the reducing agent in both cases.[15] While CO allows for the synthesis of high-quality Pt nanocubes, Pt octahedra of any size are never observed, even when the other reaction parameters are tuned (Figure S3), indicating that the Mn must be involved in the formation of octahedra. The shape evolution of octahedra is investigated by taking aliquots out of reaction after the injection of $Mn_2(CO)_{10}$ (Figure 7b). The cubes are observed within as little as 1 min. After that, the cubes gradually become truncated, and icosahedra start to form. Within 15 min, most cubes have transformed into cuboctahedra, which are intermediate between a cube and an octahedron. After 20 min, the majority of the nanocrystals have finished the transformation from cubes to octahedra.

Two possible processes would explain such transformation from cube to octahedron. It could be an etching process beginning from a cube, followed by dissolution in the ⟨111⟩ directions. Likewise, it could also be a growth process starting from a cube, with growth in the ⟨111⟩ direction. In terms of geometry, the octahedron is the dual polyhedron to the cube, namely, that the vertexes of an octahedron correspond to the faces of a cube. It can be used to describe an octahedron through the etching of a cube (Figure 7c). If this is the case, the vertex-to-vertex distance of octahedron would be equal to the edge length. The cube is also the dual polyhedron of an octahedron, visualizing the case that octahedra are grown from cubes (Figure 7d). If the original cube grows to be an octahedron, the vertex-to-vertex length of octahedron would have two times the edge length of the cube. Our observations suggest that the second "growth scenario" is operational in our case and that etching of the cubes does not occur because the octahedra have much larger lengths than the cubes. The vertex-to-vertex distance is not precisely two times the edge length of the original cubes due to the rounded vertex of the octahedra which reduces this distance. In addition, we further rule out the "etching scenario" through a "post-treatment" test, in which Pt cubes (those shown in Figure 4b) are substituted for $Pt(acac)_2$ in the synthesis of Pt octahedra. After a 30 min reaction, no morphological change of Pt cubes is observed (Figure S4b).

One possible explanation of this phenomenon (*i.e.*, cube-to-octahedron shape evolution) is that the Mn from the decomposition of $Mn_2(CO)_{10}$ selectively deposits on Pt(100) and then reduces Pt^{2+} to Pt^0, which takes the position that the Mn atom occupied. Another possibility is that Mn species (Mn atoms or ions) selectively stabilize Pt(111). A more sensitive tool would be necessary to unambiguously identify the growth

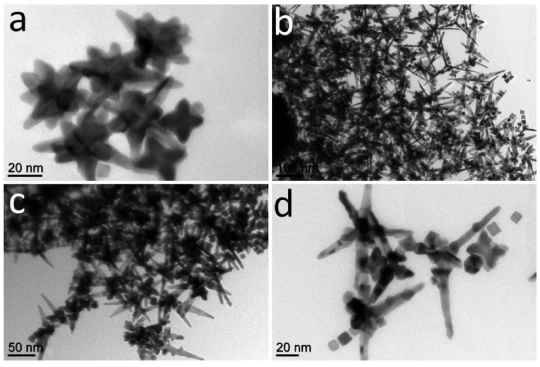

Figure 6. TEM images of (a) multipods seen after 30 min reaction and (b–d) hyper-branched Pt nanocrystals obtained after 90 min reaction.

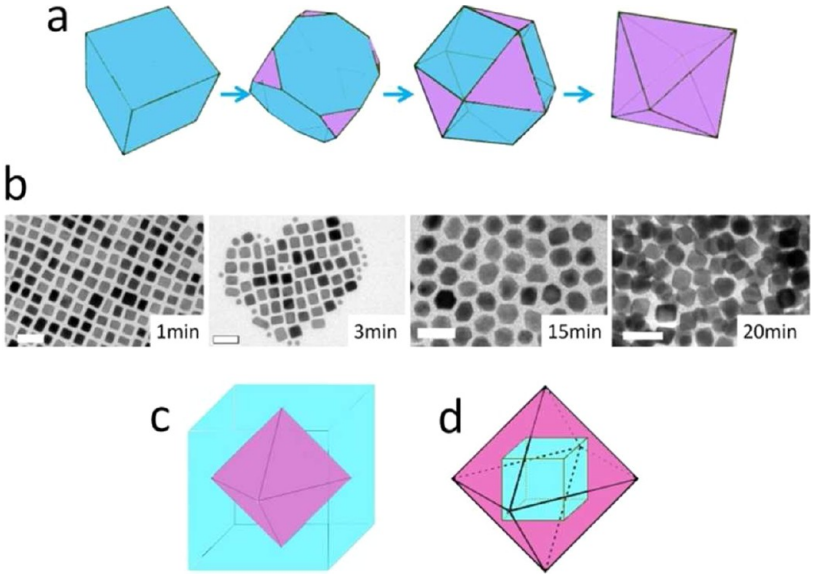

Figure 7. (a) Relation in the morphologies of cube, truncated cube, cuboctahedron, and octahedron (blue, {100}; purple, {111}). (b) TEM images of aliquots taken after the injection of Mn carbonyl solution; (c) octahedra are dual to a cube, representing the etching mechanism; (d) cube is the dual polyhedron to a octahedron, showing the way that a cube grows into an octahedron. Scale bars: 20 nm.

mechanism. Due to the lack of access to such tool, or experimental data, such as adsorption energies for Mn species on Pt(111) and Pt(100), which would confirm the selective deposition of Mn on Pt (100), we use an indirect method to determine the mechanism. We test several other metal carbonyls for the reduction of Pt to form Pt nanocrystals (Figure S5). Similar results are obtained by using $Fe(CO)_5$ or $Co_2(CO)_8$ in place of $Mn_2(CO)_{10}$. $Cr(CO)_6$ or $Re_2(CO)_{10}$ also produces Pt octahedra, but not as well-controlled as the growth observed with $Mn_2(CO)_{10}$. $W(CO)_6$ and $Mo(CO)_6$ are similar to gaseous CO, producing only Pt nanocubes. Mn and Fe powders are also tested as substitutes for carbonyls (Figure S6). The reaction with Fe powder generates some Pt octahedra, although both the quality and the quantity are low, which reinforces the fact that adding a transition metal is important for the formation of octahedra. Mn powder does not result in Pt octahedra, most likely because it fails to provide Mn^0 due to the surface oxidation. Zerovalent metals will result from the decomposition of carbonyls, but the stability of zerovalent metal is varied. The stability of the zero valence in the presented reaction system follows the order: Co, Fe > Mn > Re > Cr > W, Mo.[57−61] The ability of metal carbonyls to produce Pt octahedra also follows this trend, implying that the existence of zerovalent metal is important in the synthesis of Pt octahedra rather than that of metal ions (Figure S7). Moreover, the process is mass-transfer-limited. High-quality Pt octahedra are obtained under mild stirring (*i.e.*, 150−200 rpm), which is sufficient for the heat transfer; when the vigorous stirring (*i.e.*, >400 rpm) is employed, only cubes and worm-like product are generated (Figure S4a). This observation indicates that the growth process to form octahedra is suppressed and that, after the initial formation of cubes, the remaining Pt precursor does not grow on the cubes, but rather forms the morphology which is usually seen upon the decomposition of $Pt(acac)_2$ in benzyl ether, implying that the selective deposition of Mn is interrupted. Herein, we conclude that the $Mn_2(CO)_{10}$ has a bifunctional role in the synthesis of Pt octahedra, in which CO provides the reducing power and Mn acts as a shape-directing agent.

In the synthesis of Pt cuboctahedra (Figure 5a), the amount of $Mn_2(CO)_{10}$ used is 5 times that used in the synthesis of octahedra. When the proposed growth proceeds, the Pt precursor is depleted before the complete transformation to octahedra, thus, the final product is intermediate between the cubic and octahedral morphology. Moreover, the size of cuboctahedra is smaller than that of octahedra because the high concentration of CO and Mn produces more Pt nuclei, and thus each nanocrystal has less Pt. It follows that, if the Mn/Pt ratio is further increased to 10 times, the Mn/Pt ratio of the octahedra synthesis, the size of produced Pt nanocrystals is so small that the faceted crystal looks like a sphere (Figure 5b).

In the synthesis of branched Pt nanocrystals (tetrapods, octapods, multipods, and hyper-branched Pt nanocrystals), the common synthetic parameter is low carbonyl-to-$Pt(acac)_2$ ratio and/or long reaction time. In these cases, carbonyls are depleted before all Pt precursors are reduced to Pt^0 (monomer). After depletion of the carbonyls, the formation of monomers continues because reaction temperature is above the $Pt(acac)_2$ decomposition temperature in the presence of oleylamine. The monomers generated are consumed by the further growth of Pt nanocrystals. This creates gradients of monomer concentration. The corners of the Pt nanocrystals stick out further, thus reaching a volume of the solution that still maintains higher monomer concentration than near the surface of the rest of the nanocrystal. With more monomers reaching the corners (branches), the corners (branches) grow faster, making them reach even higher concentration of monomers and grow even faster. This phenomenon is known as branching instability and is seen in many cases of crystal growth such as growth of snow crystals.[62] The branching instability well explains the formation of tetrapods, octapods, multipods, and hyper-branched structures.

CONCLUSION

In summary, we have developed a synthetic system using $Mn_2(CO)_{10}$ to control the shape of Pt nanocrystals very precisely. In this system, high-quality Pt nanocrystals are synthesized in various morphologies, including octahedra, icosahedra, cubes, truncated cubes, cuboctahedra, spheres, tetrapods, star-shaped octapods, multipods, and hyper-branched structures. Among these morphologies, we demonstrate the first synthesis of Pt icosahedra. In addition, we first demonstrate a range of morphologies of high-quality Pt nanocrystal, which can be made at the level of material supply. The Pt nanocrystals selectively exposing {111} or {100} facets enable many interesting experiments for catalysis, such as the investigation of structure-sensitive reactions. The branched nanostructures could be useful for applications, such as surface-enhanced Raman spectroscopy (SERS).[63,64] These highly controlled Pt nanocrystals are also ideal building blocks to study the self-assembly process at nanoscale.[41,65,66]

METHODS

Synthesis. Precursor mixture is prepared by dissolving 0.08 g of $Pt(acac)_2$ in 10 mL of benzyl ether, 7.36 mL of oleylamine, and 1.25 mL of oleic acid under N_2 atmosphere. The reaction flask is then placed into a preheated oil bath. An additive solution of $Mn_2(CO)_{10}$ is injected (rapidly) into the precursor mixture at a certain temperature (injection temperature), and the reaction is allowed to be heated to a certain temperature (reaction temperature). After 30 min of reaction at the reaction temperature, the solution is cooled and the products are isolated by adding ethanol and centrifugation (post-treatment). The nanocrystals are redispersed in hexane. For the synthesis of Pt nanocrystals with

different morphologies, the details of additive solution, injection temperature, and reaction temperature are described below.

Pt Cubes. A solution of 8 mg of $Mn_2(CO)_{10}$ in 1 mL of chloroform is injected into the precursor mixture at 160 °C, and the reaction temperature is 240 °C. Synthesis of Pt cubes using CO is described in our previous report.[15]

Pt Octahedra. A solution of 8 mg of $Mn_2(CO)_{10}$ in 1 mL of chloroform is injected into the precursor mixture at 160 °C, and the reaction temperature is in the range of 210−230 °C.

Pt Truncated Cubes and Icosahedra. A solution of 8 mg of $Mn_2(CO)_{10}$ in 1 mL of chloroform is injected into the precursor mixture at 160 °C, and the reaction temperature is in the range of 190−210 °C (lower temperature produces slightly truncated cubes and higher temperature produces highly truncated cubes). After 30 min of reaction at 190−210 °C, the solution is cooled and the products are isolated by adding ethanol and centrifugation. The nanocrystals are redispersed in hexane (containing 1% oleylamine) and are separated by centrifugation. The soluble colloidal nanocrystals are mainly Pt truncated cubes, and the insoluble precipitations are mainly Pt icosahedra. Each product can be further purified by size-selective precipitation.

Pt Cuboctahedra. A solution of 40 mg of $Mn_2(CO)_{10}$ in 1 mL of chloroform is injected into the precursor mixture at 160 °C, and the reaction temperature is 200 °C.

Pt Spheres. A solution of 80 mg of $Mn_2(CO)_{10}$ in 1 mL of chloroform is injected into the reaction mixture at 160 °C, and the reaction temperature is 200 °C.

Pt Tetrapods. A solution of 24 mg of $Mn_2(CO)_{10}$ in 12 mL of benzyl ether is injected into the precursor mixture at 180 °C, and the reaction temperature is 220 °C. After post-treatment, the soluble colloidal nanocrystals are mainly Mn−Pt nanocubes, and the insoluble precipitations are mainly Pt tetrapods.

Pt Star-like Octapods (and Multipods). A solution of 4 mg of $Mn_2(CO)_{10}$ in 4 mL of benzyl ether is injected into the precursor mixture at 180 °C, and the reaction temperature is 220 °C (200 °C for multipods).

Characterizations. Transmission electron microscope (TEM) images are taken on JEOL1400 TEM at 120 kV. High-resolution TEM (HRTEM) images are taken on JEOL2010F TEM at 200 kV. Partial HRTEM images (Figures 1d and 4e) are taken using a Cs-corrected FEI Titan 80-300 at 300 kV. Quantitative elemental analyses for the composition of nanocrystals are carried out with inductively coupled plasma optical emission spectrometry (ICP-OES) on a SPECTRO GENESIS ICP spectrometer.

Conflict of Interest: The authors declare no competing financial interest.

Acknowledgment. C.B.M. and Y.J.K. acknowledge the partial support from the National Science Foundation MRSEC DMR11-20901. J.P. acknowledges the support by the Rachleff Scholars Program. X.Y. acknowledges the support from the Office of Naval Research (ONR) Multidisciplinary University Research Initiative (MURI) on Optical Metamaterials through award N00014-10-1-0942. C.B.M. thanks the Richard Perry University Professorship for the support of his supervisor role. Research carried out in part at the Center for Functional Nanomaterials (CFN), Brookhaven National Laboratory (BNL), which is supported by the U.S. Department of Energy, Office of Basic Energy Sciences, under Contract No. DE-AC02-98CH10886. We thank Charles Black (CFN, BNL) for the support at CFN, Douglas Yates at the Penn Regional Nanotechnology Facility for support in electron microscopy, and David Vann at Department of Earth and Environmental Science (University of Pennsylvania) for assistance in ICP-OES.

Supporting Information Available: TEM images presenting control experiments and XRD pattern of the major byproduct, ammonium chloride, in the synthesis using chloroform. This material is available free of charge *via* the Internet at http://pubs.acs.org.

REFERENCES AND NOTES

1. Li, Y.; Somorjai, G. A. Nanoscale Advances in Catalysis and Energy Applications. *Nano Lett.* **2010**, *10*, 2289–2295.
2. Sun, Y. G.; Xia, Y. N. Shape-Controlled Synthesis of Gold and Silver Nanoparticles. *Science* **2002**, *298*, 2176–2179.
3. Xia, Y. N.; Xiong, Y. J.; Lim, B.; Skrabalak, S. E. Shape-Controlled Synthesis of Metal Nanocrystals: Simple Chemistry Meets Complex Physics?. *Angew. Chem., Int. Ed.* **2009**, *48*, 60–103.
4. Tao, A. R.; Habas, S.; Yang, P. Shape Control of Colloidal Metal Nanocrystals. *Small* **2008**, *4*, 310–325.
5. Zhang, J.; Yang, H.; Fang, J.; Zou, S. Synthesis and Oxygen Reduction Activity of Shape-Controlled Pt_3Ni Nanopolyhedra. *Nano Lett.* **2010**, *10*, 638–644.
6. Wang, C.; van der Vilet, D.; Chang, K.-C.; You, H.; Strmcnik, D.; Schlueter, J. A.; Markovic, N. M.; Stamenkovic, V. R. Monodisperse Pt_3Co Nanoparticles as a Catalyst for the Oxygen Reduction Reaction: Size-Dependent Activity. *J. Phys. Chem. C* **2009**, *113*, 19365–19368.
7. Liu, Q. S.; Yan, Z.; Henderson, N. L.; Bauer, J. C.; Goodman, D. W.; Batteas, J. D.; Schaak, R. E. Synthesis of CuPt Nanorod Catalysts with Tunable Lengths. *J. Am. Chem. Soc.* **2009**, *131*, 5720–5721.
8. Buck, M. R.; Bondi, J. F.; Schaak, R. E. A Total-Synthesis Framework for the Construction of High-Order Colloidal Hybrid Nanoparticles. *Nat. Chem.* **2012**, *4*, 37–44.
9. Ye, X.; Collins, J. E.; Kang, Y. J.; Chen, J.; Chen, D. T. N.; Yodh, A. G.; Murray, C. B. Morphologically Controlled Synthesis of Colloidal Upconversion Nanophosphors and Their Shape-Directed Self-Assembly. *Proc. Natl. Acad. Sci. U.S.A.* **2010**, *107*, 22430–22435.
10. Sau, T. K.; Rogach, A. L. Nonspherical Noble Metal Nanoparticles: Colloid-Chemical Synthesis and Morphology Control. *Adv. Mater.* **2010**, *22*, 1781–1804.
11. Bratlie, K. M.; Lee, H.; Komvopoulos, K.; Yang, P. D.; Somorjai, G. A. Platinum Nanoparticle Shape Effects on Benzene Hydrogenation Selectivity. *Nano Lett.* **2007**, *7*, 3097–3101.
12. Tian, N.; Zhou, Z. Y.; Sun, S. G.; Ding, Y.; Wang, Z. L. Synthesis of Tetrahexahedral Platinum Nanocrystals with High-Index Facets and High Electro-oxidation Activity. *Science* **2007**, *316*, 732–735.
13. Solla-Gullon, J.; Vidal-Iglesias, F. J.; Lopez-Cudero, A.; Garnier, E.; Feliu, J. M.; Aldaza, A. Shape-Dependent Electrocatalysis: Methanol and Formic Acid Electrooxidation on Preferentially Oriented Pt Nanoparticles. *Phys. Chem. Chem. Phys.* **2008**, *10*, 3689–3698.
14. Kang, Y. J.; Murray, C. B. Synthesis and Electrocatalytic Properties of Cubic Mn−Pt Nanocrystals (Nanocubes). *J. Am. Chem. Soc.* **2010**, *132*, 7568–7569.
15. Kang, Y. J.; Ye, X. C.; Murray, C. B. Size- and Shape-Selective Synthesis of Metal Nanocrystals and Nanowires Using CO as a Reducing Agent. *Angew. Chem., Int. Ed.* **2010**, *49*, 6156–6159.
16. Wang, D. Y.; Kang, Y. J.; Doan-Nguyen, V.; Chen, J.; Kungas, R.; Wieder, N. L.; Bakhmutsky, K.; Gorte, R. J.; Murray, C. B. Synthesis and Oxygen Storage Capacity of Two-Dimensional Ceria Nanocrystals. *Angew. Chem., Int. Ed.* **2011**, *50*, 4378–4381.
17. Kang, Y. J.; Qi, L.; Li, M.; Diaz, R. E.; Su, D.; Adzic, R. R.; Stach, E.; Li, J.; Murray, C. B. Highly Active Pt_3Pb and Core−Shell Pt3Pb−Pt Electrocatalysts for Formic Acid Oxidation. *ACS Nano* **2012**, *6*, 2818–2825.
18. Wang, C.; Chi, M.; Li, D.; Strmcnik, D.; van der Vliet, D.; Wang, G.; Komanicky, V.; Chang, K.-C.; Paulikas, A. P.; Tripkovic, D.; *et al.* Design and Synthesis of Bimetallic Electrocatalyst with Multilayered Pt-Skin Surfaces. *J. Am. Chem. Soc.* **2011**, *133*, 14396–14403.
19. Wang, C.; van der Vliet, D.; More, K. L.; Zaluzec, N. J.; Peng, S.; Sun, S. H.; Daimon, H.; Wang, G. F.; Greeley, J.; Pearson, J.; et al. Multimetallic Au/$FePt_3$ Nanoparticles as Highly Durable Electrocatalyst. *Nano Lett.* **2011**, *11*, 919–926.
20. Kang, Y.; Pyo, J. B.; Ye, X. C.; Gordon, T. R.; Murray, C. B. Synthesis, Shape Control, and Methanol Electro-oxidation Properties of Pt−Zn Alloy and Pt_3Zn Intermetallic Nanocrystals. *ACS Nano* **2012**, *6*, 5642–5647.
21. Aiken, J. D.; Finke, R. G. A Review of Modern Transition-Metal Nanoclusters: Their Synthesis, Characterization, and Applications in Catalysis. *J. Mol. Catal. A: Chem.* **1999**, *145*, 1–44.
22. Xiong, Y. J.; McLellan, J. M.; Chen, J. Y.; Yin, Y. D.; Li, Z. Y.; Xia, Y. N. Kinetically Controlled Synthesis of Triangular and

Hexagonal Nanoplates of Palladium and Their SPR/SERS Properties. *J. Am. Chem. Soc.* **2005**, *127*, 17118–17127.
23. Wiley, B. J.; Im, S. H.; Li, Z.-Y.; McLellan, J.; Siekkinen, A.; Xia, Y. Maneuvering the Surface Plasmon Resonance of Silver Nanostructures through Shape-Controlled Synthesis. *J. Phys. Chem. B* **2006**, *110*, 15666–15675.
24. Wiley, B. J.; Chen, Y.; McLellan, J. M.; Xiong, Y.; Li, Z.-Y.; Ginger, D.; Xia, Y. Synthesis and Optical Properties of Silver Nanobars and Nanorice. *Nano Lett.* **2007**, *7*, 1032–1036.
25. Tao, A.; Sinsermsuksakul, P.; Yang, P. Tunable Plasmonic Lattices of Silver Nanocrystals. *Nat. Nanotechnol.* **2007**, *2*, 435–440.
26. Chen, J.; Dong, A. G.; Cai, J.; Ye, X. C.; Kang, Y. J.; Kikkawa, J. M.; Murray, C. B. Collective Dipolar Interactions in Self-Assembled Magnetic Binary Nanocrystal Superlattice Membranes. *Nano Lett.* **2010**, *10*, 5103–5108.
27. Dong, A. G.; Chen, J.; Vora, P. M.; Kikkawa, J. M.; Murray, C. B. Binary Nanocrystal Superlattice Membranes Self-Assembled at the Liquid–Air Interface. *Nature* **2010**, *466*, 474–477.
28. Sun, S. H.; Murray, C. B.; Weller, D.; Folks, L.; Moser, A. Monodisperse FePt Nanoparticles and Ferromagnetic FePt Nanocrystal Superlattices. *Science* **2000**, *287*, 1989–1992.
29. Wang, X. D.; Summers, C. J.; Wang, Z. L. Large-Scale Hexagonal-Patterned Growth of Aligned ZnO Nanorods for Nano-optoelectronics and Nanosensor Arrays. *Nano Lett.* **2004**, *4*, 423–426.
30. Ahmadi, T. S.; Wang, Z. L.; Green, T. C.; Henglein, A.; ElSayed, M. A. Shape-Controlled Synthesis of Colloidal Platinum Nanoparticles. *Science* **1996**, *272*, 1924–1926.
31. Gillespie, W. D.; Herz, R. K.; Petersen, E. E.; Somorjai, G. A. The Structure Sensitivity of *n*-Heptane Dehydrocyclization and Hydrogenolysis Catalyzed by Platinum Single Crystals at Atmospheric Pressure. *J. Catal.* **1981**, *70*, 147–159.
32. Herz, R. K.; Gillespie, W. D.; Petersen, E. E.; Somorjai, G. A. The Structure Sensitivity of Cyclohexane Dehydrogenation and Hydrogenolysis Catalyzed by Platinum Single Crystal at Atmospheric pressure. *J. Catal.* **1981**, *67*, 371–386.
33. Spencer, N. D.; Schoonmaker, R. C.; Somorjai, G. A. Iron Single-Crystals as Ammonia-Synthesis Catalysts—Effect of Surface–Structure on Catalyst Activity. *J. Catal.* **1982**, *74*, 129–135.
34. Zaera, F.; Somorjai, G. A. Reaction of Ethane with Deuterium over Platinum(111) Single-Crystal Surfaces. *J. Phys. Chem.* **1985**, *89*, 3211–3216.
35. Somorjai, G. A.; Carrazza, J. Structure Sensitivity of Catalytic Reactions. *Ind. Eng. Chem. Fundam.* **1986**, *25*, 63–69.
36. Ren, J.; Tilley, R. D. Shape-Controtled Growth of Platinum Nanoparticles. *Small* **2007**, *3*, 1508–1512.
37. Wang, Z. L.; Ahmad, T. S.; ElSayed, M. A. Steps, Ledges and Kinks on the Surfaces of Platinum Nanoparticles of Different Shapes. *Surf. Sci.* **1997**, *380*, 302–310.
38. Narayanan, R.; El-Sayed, M. A. Shape-Dependent Catalytic Activity of Platinum Nanoparticles in Colloidal Solution. *Nano Lett.* **2004**, *4*, 1343–1348.
39. Huang, X.; Zhao, Z.; Fan, J.; Tan, Y.; Zheng, N. Amine-Assisted Synthesis of Concave Polyhedral Platinum Nanocrystals Having {411} High-Index Facets. *J. Am. Chem. Soc.* **2011**, *133*, 4718–4721.
40. Lee, I.; Delbecq, F.; Morales, R.; Albiter, M. A.; Zaera, F. Tuning Selectivity in Catalysis by Controlling Particle Shape. *Nat. Mater.* **2009**, *8*, 132–138.
41. Henzie, J.; Gruenwald, M.; Widmer-Cooper, A.; Geissler, P. L.; Yang, P. Self-Assembly of Uniform Polyhedral Silver Nanocrystals into Densest Packings and Exotic Superlattices. *Nat. Mater.* **2012**, *11*, 131–137.
42. Habas, S. E.; Lee, H.; Radmilovic, V.; Somorjai, G. A.; Yang, P. Shaping Binary Metal Nanocrystals through Epitaxial Seeded Growth. *Nat. Mater.* **2007**, *6*, 692–697.
43. Lim, S. I.; Ojea-Jimenez, I.; Varon, M.; Casals, E.; Arbiol, J.; Puntes, V. Synthesis of Platinum Cubes, Polypods, Cuboctahedrons, and Raspberries Assisted by Cobalt Nanocrystals. *Nano Lett.* **2010**, *10*, 964–973.
44. Wang, C.; Daimon, H.; Lee, Y.; Kim, J.; Sun, S. Synthesis of Monodisperse Pt Nanocubes and Their Enhanced Catalysis for Oxygen Reduction. *J. Am. Chem. Soc.* **2007**, *129*, 6974–6975.
45. Ren, J. T.; Tilley, R. D. Preparation, Self-Assembly, and Mechanistic Study of Highly Monodispersed Nanocubes. *J. Am. Chem. Soc.* **2007**, *129*, 3287–3291.
46. Zhang, J.; Fang, J. Y. A General Strategy for Preparation of Pt 3d-Transition Metal (Co, Fe, Ni) Nanocubes. *J. Am. Chem. Soc.* **2009**, *131*, 18543–18547.
47. Song, H.; Kim, F.; Connor, S.; Somorjai, G. A.; Yang, P. D. Pt Nanocrystals: Shape Control and Langmuir–Blodgett Monolayer Formation. *J. Phys. Chem. B* **2005**, *109*, 188–193.
48. Lee, H.; Habas, S. E.; Kweskin, S.; Butcher, D.; Somorjai, G. A.; Yang, P. D. Morphological Control of Catalytically Active Platinum Nanocrystals. *Angew. Chem., Int. Ed.* **2006**, *45*, 7824–7828.
49. Xiong, Y. J.; McLellan, J. M.; Yin, Y. D.; Xia, Y. N. Synthesis of Palladium Icosahedra with Twinned Structure by Blocking Oxidative Etching with Citric Acid or Citrate Ions. *Angew. Chem., Int. Ed.* **2007**, *46*, 790–794.
50. Li, C. C.; Sato, R.; Kanehara, M.; Zeng, H. B.; Bando, Y.; Teranishi, T. Controllable Polyol Synthesis of Uniform Palladium Icosahedra: Effect of Twinned Structure on Deformation of Crystalline Lattices. *Angew. Chem., Int. Ed.* **2009**, *48*, 6883–6887.
51. Ling, T.; Xie, L.; Zhu, J.; Yu, H. M.; Ye, H. Q.; Yu, R.; Cheng, Z.; Liu, L.; Yang, G. W.; Cheng, Z. D.; *et al.* Icosahedral Face-Centered Cubic Fe Nanoparticles: Facile Synthesis and Characterization with Aberration-Corrected TEM. *Nano Lett.* **2009**, *9*, 1572–1576.
52. Yavuz, M. S.; Li, W. Y.; Xia, Y. N. Facile Synthesis of Gold Icosahedra in an Aqueous Solution by Reacting $HAuCl_4$ with *N*-Vinyl Pyrrolidone. *Chem.—Eur. J.* **2009**, *15*, 13181–13187.
53. Kuai, L.; Geng, B. Y.; Wang, S. Z.; Zhao, Y. Y.; Luo, Y. C.; Jiang, H. Silver and Gold Icosahedra: One-Pot Water-Based Synthesis and Their Superior Performance in the Electrocatalysis for Oxygen Reduction Reactions in Alkaline Media. *Chem.—Eur. J.* **2011**, *17*, 3482–3489.
54. Kim, F.; Connor, S.; Song, H.; Kuykendall, T.; Yang, P. D. Platonic Gold Nanocrystals. *Angew. Chem., Int. Ed.* **2004**, *43*, 3673–3677.
55. Wu, J.; Qi, L.; You, H.; Gross, A.; Li, J.; Yang, H. Icosahedral Platinum Alloy Nanocrystals with Enhanced Electrocatalytic Activities. *J. Am. Chem. Soc.* **2012**, *134*, 11880–11883.
56. Xu, D.; Liu, Z. P.; Yang, H. Z.; Liu, Q. S.; Zhang, J.; Fang, J. Y.; Zou, S. Z.; Sun, K. Solution-Based Evolution and Enhanced Methanol Oxidation Activity of Monodisperse Platinum–Copper Nanocubes. *Angew. Chem., Int. Ed.* **2009**, *48*, 4217–4221.
57. Puntes, V. F.; Krishnan, K. M.; Alivisatos, A. P. Colloidal Nanocrystal Shape and Size Control: The Case of Cobalt. *Science* **2001**, *291*, 2115–2117.
58. Lacroix, L. M.; Huls, N. F.; Ho, D.; Sun, X. L.; Cheng, K.; Sun, S. H. Stable Single-Crystalline Body Centered Cubic Fe Nanoparticles. *Nano Lett.* **2011**, *11*, 1641–1645.
59. Bondi, J. F.; Oyler, K. D.; Ke, X.; Schiffer, P.; Schaak, R. E. Chemical Synthesis of Air-Stable Manganese Nanoparticles. *J. Am. Chem. Soc.* **2009**, *131*, 9144–9145.
60. Hayward, C. M. T.; Shapley, J. R. Direct Synthesis and Interconversion of Large Rhenium Carbonyl Clusters. *Organometallics* **1988**, *7*, 448–452.
61. Hughes, S. J.; Moss, J. R.; Naidoo, K. J.; Kelly, J. F.; Batsanov, A. S. Force-Field Parameterisation, Synthesis and Crystal Structure of a Novel Tricarbonylchromium Arene Complex. *J. Organomet. Chem.* **1999**, *588*, 176–185.
62. Libbrecht, K. G. The Physics of Snow Crystals. *Rep. Prog. Phys.* **2005**, *68*, 855–895.
63. Khoury, C. G.; Vo-Dinh, T. Gold Nanostars For Surface-Enhanced Raman Scattering: Synthesis, Characterization and Optimization. *J. Phys. Chem. C* **2008**, *112*, 18849–18859.
64. Sau, T. K.; Rogach, A. L.; Jaeckel, F.; Klar, T. A.; Feldmann, J. Properties and Applications of Colloidal Nonspherical Noble Metal Nanoparticles. *Adv. Mater.* **2010**, *22*, 1805–1825.

65. Rogach, A. L.; Talapin, D. V.; Shevchenko, E. V.; Kornowski, A.; Haase, M.; Weller, H. Organization of Matter on Different Size Scales: Monodisperse Nanocrystals and Their Superstructures. *Adv. Funct. Mater.* **2002**, *12*, 653–664.
66. Claridge, S. A.; Castleman, A. W., Jr.; Khanna, S. N.; Murray, C. B.; Sen, A.; Weiss, P. S. Cluster-Assembled Materials. *ACS Nano* **2009**, *3*, 244–255.